Journal of Japan Association for Earthquake Engineering, Vol. 18, No. 3, 2018

SIMPLE EVALUATION INDEX FOR STRUCTURAL DAMAGE OF HIGH-RISE REINFORCED CONCRETE BUILDINGS DUE TO LONG-PERIOD STRONG GROUND MOTION

Hirotoshi UEBAYASHI [1], Masayuki NAGANO [2], Katsuhiro KAMAE [3], and Hidenori KAWABE [4]

[1] Member of JAEE, Associate Professor, Research Reactor Institute, Kyoto University, Dr. Eng., uebayash@rri.kyoto-u.ac.jp
[2] Member of JAEE, Professor, Dept. of Architecture, Tokyo University of Science, Dr. Eng., nagano-m@rs.noda.tus.ac.jp
[3] Member of JAEE, Professor, Research Reactor Institute, Kyoto University, Dr. Eng., kamae@rri.kyoto-u.ac.jp
[4] Member of JAEE, Associate Professor, Graduate School of Engineering Osaka University, Dr. Eng., kawabe@arch.eng.osaka-u.ac.jp

ABSTRACT: Simple evaluation of the degree of structural damage suffered by high-rise RC buildings after being subjected to strong ground motions is extremely important. For a large number of high-rise RC residential buildings for which strong-motion measurements or observations of microtremors before and after earthquakes have not been carried out, we developed a benchmark indicator allowing simple characterization—based on pseudovelocity response spectra for strong-motion records measured at ground points close to the building, as well as re-created waves and other data—of peak inter-story drift ratio values expected in a future major earthquake.

Key Words: High-Rise RC Buildings, Simple Structural-Damage Indicator, Equivalent SDOF Model, Elasto-Plastic Response Analysis

1. INTRODUCTION

At present, Japan has over 1300 high-rise (taller than 60 m) residential buildings that are predominantly built with reinforced concrete (RC) (hereinafter referred to as "high-rise RC structures")[1)], and this number is on track to rise in the future. Most of these buildings are located in the Tokyo metropolitan area or the Kansai region, which would be heavily affected by great inland crustal earthquakes or a megathrust earthquake at the Nankai trough—one of the events identified for consideration by the Central Disaster Management Council[2)]. Moreover, examples have been presented in which the response spectra for the seismic ground motions predicted to arise from earthquakes of this type significantly exceed the standard design response spectrum for safety limit criteria defined for engineering bedrock in Japan (constant level 80 cm/s) for periods of about 1 s or longer (one example is given in Ref. 3). Thus, early and wide-ranging assessments of the degree of damage suffered by buildings (maximum deformation and maximum stiffness degradation rate) are

thought to be important components for devising Mansion Life Continuity Plans (MLCPs) for residents of high-rise RC buildings that may be damaged by major earthquakes in the future.

To date, numerous studies have estimated the degree of damage suffered by buildings in earthquakes by analyzing severe earthquake records at the base and top of the buildings. However, strong-motion measurements are not carried out for many high-rise RC structures, creating a need for methods for assessing structural damage that do not depend on strong-motion records for buildings. Hida et al.[4] analyzed the results of surveys—in which residents of multiple buildings damaged in the 2011 off the Pacific coast of Tohoku Earthquake (the *Tohoku-Oki earthquake*) were asked to describe personal experiences and indoor damage—and demonstrated a clear relationship between the appearance of cracks and tears in wallpaper and peak inter-story drift ratios (PIDRs) obtained from strong-motion records. However, PIDRs for the buildings surveyed were less than around 1/150, and some sort of extrapolation is needed for stronger earthquakes.

Methods that use changes in the natural period of a building's microtremors before and after earthquakes to estimate maximum stiffness degradation rates and PIDRs during strong motions may also be considered[5]. These are simple methods that do not require estimates of a building's input motion or analysis of its response, but they do require that a building's dynamic properties due to microtremors have been characterized in advance, before a strong earthquake is experienced. On the other hand, one may also consider methods that use design information to identify the portions of buildings most likely to suffer damage under elasto-plastic response, then use the extent of damage suffered by those regions after an earthquake to estimate the extent of the damage suffered by the building as a whole. However, such methods presumably require not only a clear determination of the relevant regions, but also a quantification of the structural damage they suffer and a quantitative understanding of how damage to these regions relates to damage suffered by the building as a whole.

Recently, there has been a trend in which strong-motion monitoring networks at ground level have expanded to cover wider geographical areas—primarily in major metropolitan areas—and have grown more dense. Information recorded by various monitoring organizations is increasingly aggregated and organized in a unified framework, converted to database form, and made publicly available via the Web. Moreover, three-dimensional underground velocity structural models have been constructed for major metropolitan areas, allowing surface-level reconstruction of strong earthquake dynamics in the early stages following the occurrence of a major earthquake. These advances have made it possible to acquire an understanding of the input ground motion affecting high-rise structures in the early stages after earthquakes. Thus, the development of a simple evaluation index (hereafter referred to as a simple benchmark indicator) that would allow simple assessment of the extent of damage suffered by buildings from measurements or estimates of ground motions around the building—without conducting strong-motion monitoring inside buildings, for which it is difficult to obtain the consent of building owners—would be extremely valuable. In this paper, we derive a benchmark indicator that allows—for high-rise RC residential structures built to conventional specifications, without seismic-isolation or earthquake-limiting devices—simple estimation of PIDR values (averaged over all stories) during strong earthquakes from input ground motion.

2. DYNAMIC PROPERTIES OF HIGH-RISE RC STRUCTURES IN ELASTO-PLASTIC RESPONSE

2.1 Input ground motion levels in the 1995 Hyogoken-Nambu and 2011 Tohoku-Oki earthquakes

Striking nonlinear response patterns were observed in multiple high-rise RC structures during both the Mw 6.9 earthquake that struck the southern region of Japan's Hyogo prefecture in 1995 (the *Hyogoken-Nambu earthquake*) and the Mw 9.0 earthquake off the coast of Japan's Tohoku region in 2011 (the *Tohoku-Oki earthquake*)[6)-10)]. In particular, the application of system-identification techniques to time-series data for RC structures in the Kanto and Kansai regions indicated that, although the natural periods of buildings increased together with their maximum amplitude response, the natural periods did not return to their initial values after the earthquake, indicating decreased

stiffness[9), 11)]. Note that, of the 14 buildings analyzed in Refs. 9 and 11, all but one was an RC structure [the only exception was a single concrete-filled steel-tube (CFT) structure]. The responses of these 13 high-rise RC structures to the two earthquakes, and the damage they suffered, rank among the most significant in all of Japan, and observations made in the interior of these buildings thus yield extremely valuable information on strong-earthquake behavior. As discussed below, we use the relationship between maximum response and stiffness degradation obtained from this observational data to establish skeleton curves for the evaluation model proposed in this paper. Before turning to this discussion, we first make a number of observations regarding input ground motion in these two earthquakes.

Among the seismic records obtained at ground level for the two earthquakes, a comparison of waveforms observed in Nagata Ward of Kobe City during the Hyogoken-Nambu earthquake and in Shinjuku City of Tokyo during the Tohoki-Oki earthquake[12), 13)] reveals clear differences in scale, epicentral distance, and progression of fault destruction versus the temporal duration and the maximum velocity of ground motion (Fig. 1a). Fig. 1b shows pseudovelocity response spectra (pSv, damping factor h=5%) for these two sites and for two additional sites: a region of northwest Osaka City for the Hyogoken-Nambu earthquake and a region outside of Soka City for the Tohoku-Oki earthquake. From this figure, we can see that, for the Hyogoken-Nambu earthquake in the region from northwest Osaka City to the Kobe area, values for periods from just below 1 s to just below 3 s vary between approximately 1 to more than 2 times the values of indicated spectra for the safety limit (80 cm/s). On the other hand, for the Kanto plain in the Tohoku-Oki earthquake, values for periods of about 1 s and above lie between the indicated spectra for the damage limit (16 cm/s) and the safety limit (80 cm/s).

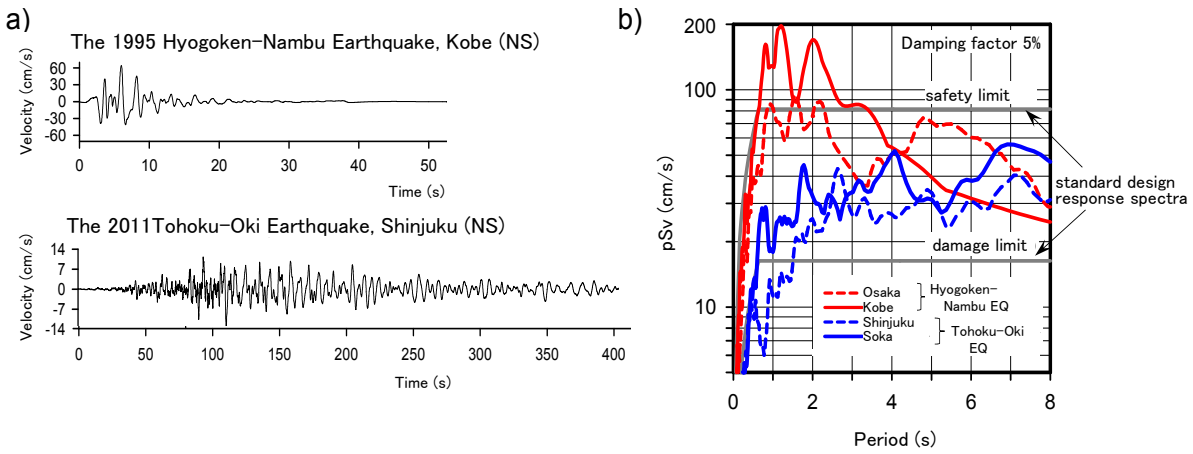

Fig. 1 Examples of velocity waveforms observed during the Hyogoken-Nambu and Tohoku-Oki earthquakes (a) and pseudovelocity response spectra (b).

2.2 Establishing a model of dynamic properties

Analysis of strong-motion records for the 13 high-rise RC structures in the two major earthquakes discussed above reveals that, in a model in which buildings are approximated by an equivalent single-degree-of-freedom (SDOF) system, skeleton curves may be approximated as a two-branch linear model[9), 11)]. In what follows, we describe the procedure for setting parameters in an elasto-plastic SDOF model based on these results. Figs. 2a,b show the relationship between force and displacement in terms of the PIDR (for which we use the symbol γ) and the dimensionless horizontal force, as shown in Fig. 2c. Fig. 2a corresponds to the elastic state, while Fig. 2b corresponds to the state believed to follow the emergence of cracks in the beam endpoints of the structure. For both cases, we show the results of analysis of observation records (symbols ○, ●) and the results of least-squares regression analysis. Here, the dimensionless horizontal force $q(\gamma)$ is computed by multiplying the

PIDR at maximum deformation by the square of the ratios of the natural periods for the initial stiffness (k_1), shown in Fig. 2d, and for the equivalent stiffness k_e at the time of maximum response, i.e. $q=(T_1/T_e)^2\,\gamma$). This may be determined from the observational records discussed above. We determine the coefficients a and b from a regression analysis of the relationship between q and γ:

$$q(\gamma) = Q/(kH) = b\gamma + a \tag{1}$$

where Q is the horizontal force, k is the skeleton-curve stiffness, and H is the equivalent height. Our results indicate that, for PIDR values below the elastic limit ($\gamma<\gamma_0$), b=0.87, which is slightly lower than the true value of 1.

On the other hand, for PIDR values ($\gamma_0<\gamma$) above the elastic limit (after the emergence of cracks in the beam endpoint), we find $a=4.0\times10^{-4}$, b=0.32 (Fig. 2b). The value of b here corresponds to the ratio k_2/k_1, where k_1 is the initial stiffness (first branch of skeleton curve) and k_2 is the stiffness beyond the elastic limit (second branch). These regression results signify that the stiffness degradation is almost entirely determined by the maximum response (PIDR), independent of the duration of ground motion (Fig. 1). Also, from the intersection of the true value of Fig. 2a with the regression line of Fig. 2b, we find the PIDR in the elastic limit to be 6.0×10^{-4}. Based on these findings, we determine values up to the second branch in the skeleton curve for the various parameters in the Takeda model, which is commonly used to model restoring-force characteristics for RC structures, and the results are shown in

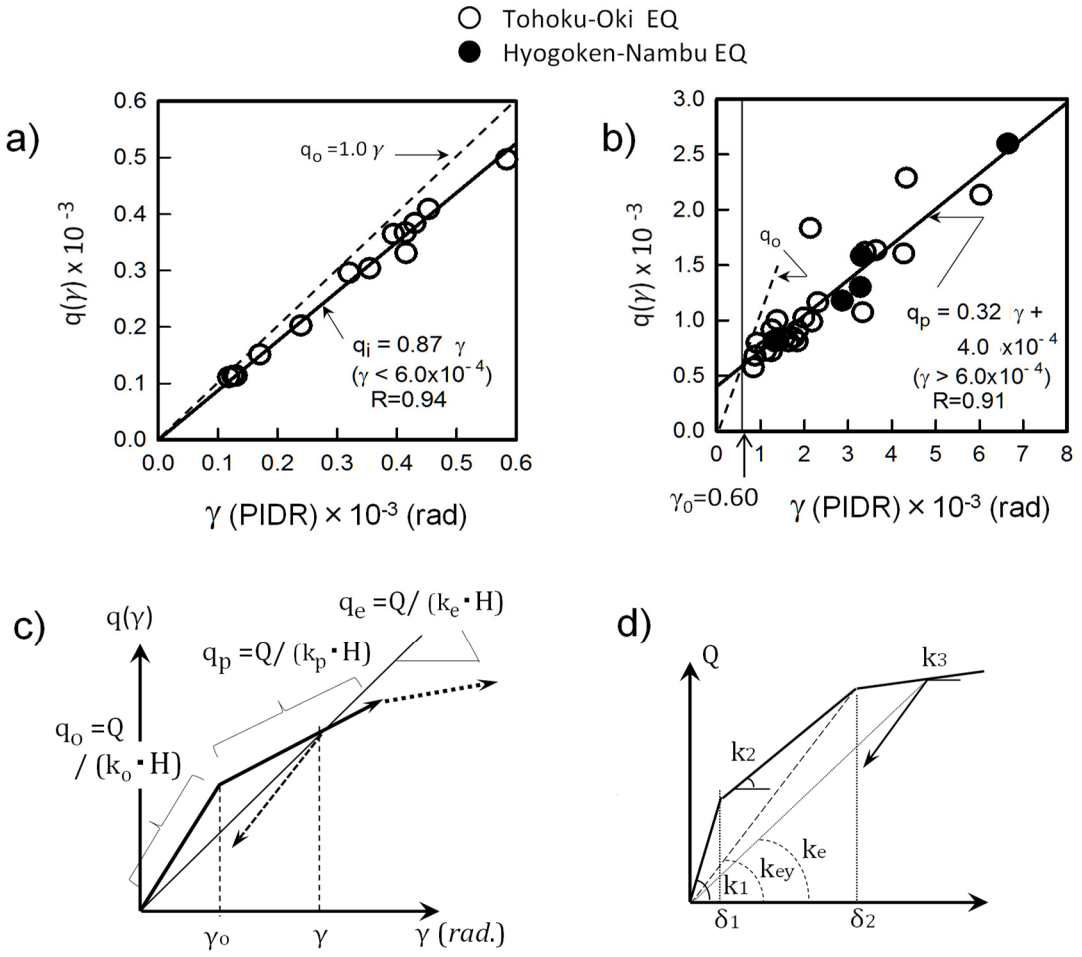

Fig. 2 Relationship between dimensionless horizontal force and PIDR (a-c) and skeleton curves for equivalent SDOF model (d).

Fig. 2d. Based on the results of analyses of earthquake observational records for small-amplitude response, and using an instantaneous-stiffness proportionality model, we set the value of the damping factor in the elastic-response regime to 2%. On the other hand, for the PIDR at the second inflection point, we choose the value 8.6×10^{-3} based on design data (such as Ref. 14). This is based on the observation that, in Fig. 2b, the observational plot is distributed near the regression line at least as far as values of about 8×10^{-3}. For the third branch, we use the value $0.01k_1$ typically used for design work. For the natural period of our building model, we use the value 2 s, the mean value for the buildings in the strong-earthquake-record analysis described above. Analytical results and discussion for other values of the natural period are presented later in this paper.

2.3 Discussion of the usefulness of our model

In the previous section, we discussed the reduction of a high-rise RC structure to an equivalent SDOF model and the choice of parameters affecting the dynamic properties of this model. In this section, we address two further points relevant to this discussion: **(1)** the impact of higher-order vibrational modes on PIDR, a quantity important for characterizing the extent of damage suffered by RC buildings, and **(2)** how the various parameters described above are positioned with respect to fluctuations from building to building in multiple-mass-point design models.

Addressing item **(1)** first, we note that, as the amplitude of a high-rise RC structure increases, the beams on each story are the first structural elements to yield; common design practice is to adopt an overall-collapse structure in which no individual story exhibits particularly prominent stiffness degradation. This is what allows responses to ground motion to be characterized with reasonable accuracy based on a reduced model consisting of just a SDOF that properly captures the relationship of deformation and stiffness degradation for the building as a whole. Among the 13 buildings with strong-motion records discussed above, in one case—namely, a building in Soka City that experienced the Tohoku-Oki earthquake, for which input ground motion (observed records at the base of the building) delivered a relatively large amount of power in a relatively short period of time (solid blue line in Fig. 1b)—response to the same earthquake has been analyzed using a multiple-mass-point design model[15]. The results of this analysis indicate that first-order modes make the dominant contributions to the PIDRs for all stories. Moreover, the Kanto and Osaka plains—in which many high-rise RC structures exist—contain thick sedimentary layers with thicknesses of several hundred meters or more, which generally feature prominent ground motion in the long-period band of 2 s and above. Considering the properties of a major earthquake (M7 or greater) arising along the Nankai trough or in an inland region (with the dominant period estimated empirically from the area of the region in which a strong earthquake might arise), we may expect that components with periods near 2 s and above will be key contributors to the ground motion input to the plains. On the other hand, it has been shown that the ductility factor of multi-story structures—for several standard waves commonly used in design, due to input waves with maximum velocity amplitude standardized at 50 cm/s— may be predicted by analyzing the elasto-plastic response of an equivalent SDOF system, although this example concerned high-rise steel structures[16]. Based on these findings, we conclude it is highly likely that stiffness degradation (damage) due to a major earthquake in high-rise RC structures located in regions with thick sedimentary layers can be approximately characterized based on the contributions of first-order modes alone.

As for item **(2)**, among the parameters set for skeleton curves we consider three quantities: the PIDR in the elastic limit, the ratio of the stiffness beyond the elastic limit to the initial stiffness (k_2/k_1), and the ratio of the equivalent stiffness at the second inflection point to the initial stiffness (k_{ey}/k_1). The upper plots in Figs. 3a,b,c show the distribution of story-to-story and building-to-building variations in these quantities as obtained from design information for 9 of the 13 buildings discussed above. In these plots, building height is normalized by maximum height. For some of the buildings in which the stiffness in the two horizontal directions differs slightly, we have plotted results for both directions. Based on these data distributions, we obtained the mean value of various quantities in the height direction (empty circles in lower plots), and then computed the mean and the mean ± standard

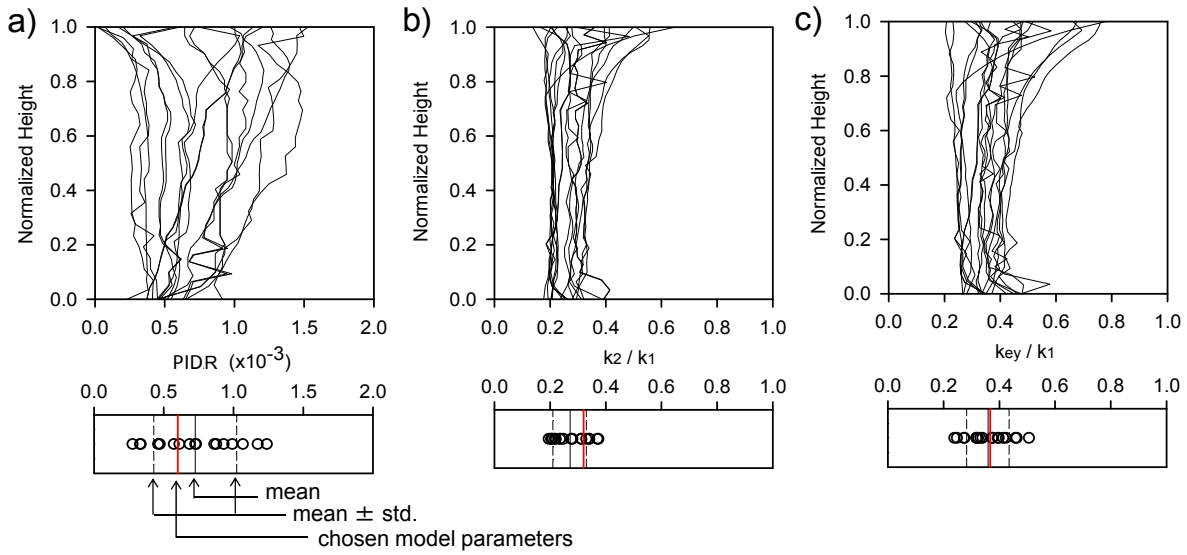

Fig. 3 Elastic-limit PIDR (a) and stiffness ratios (b,c) obtained from the design model. In each case, the upper figure shows the distribution of values in the height direction for each building, while the lower figure shows mean values of the height-direction values for each building.

deviation of all empty circles (for each building) (solid and dashed black lines). Based on these results, we can think of the values we chose for the model parameters (red lines) as mean values, averaged over all buildings. Building-to-building fluctuations in parameter values may affect variations in the benchmark indicator we introduce later to characterize the extent of damage. However, fluctuations in building response, as characterized from observational records (Figs. 2a,b) are relatively small (correlation coefficient above 0.9) compared to building-to-building fluctuations (Fig. 3). On the other hand, as discussed in Section 3.2 below, fluctuations in building response due to differences in amplitude vs. frequency characteristics among sites of input ground motion are extremely large in the elasto-plastic response regime. Based on these observations, we conclude that building-to-building fluctuations in dynamic properties for the high-rise RC structures discussed above exhibit minimal impact on the benchmark indicator for structural damage that we derive below. Next, we note that the design the base shear coefficient—one piece of design information that is publicly available—has been used to position the 9 buildings analyzed in this study vis-a-vis other high-rise RC buildings in terms of design tolerance[17]. Based on this finding, it has been shown that the relationship between the natural period and the base shear coefficient agrees well with the regression equations obtained for a large number of high-rise RC structures. This suggests that the dynamic properties we use in this study should also reflect mean design values for existing high-rise buildings beyond the 9 we consider here.

3. A BENCHMARK INDICATOR FOR CHARACTERIZING THE MAXIMUM RESPONSE OF HIGH-RISE RC BUILDINGS FROM INFORMATION ON INPUT GROUND MOTION

3.1 Predicted ground motions from a hypothetical Nankai earthquake

To calculate the elasto-plastic response for the equivalent SDOF model described above, we applied a Butterworth low-pass filter with flat response at 2 s and above to input ground motion from wavefields[18] predicted by the Osaka sedimentary basin model (Fig. 4a) for a hypothetical Nankai earthquake (Fig. 4b). We calculated values for a total of 1,868 points (at 800 m intervals) indicated by dots in Fig. 4b. For the primary fault parameters in the hypothetical Nankai earthquake, we used the following values: total fault area 35,800 km^2, asperities 2,672 km^2 (Asp1), 1,336 km^2 (Asp2), 1,336 km^2 (Asp3), moment magnitude Mw 8.6, and mean slip 5.7 m. The hypocenter, which heavily

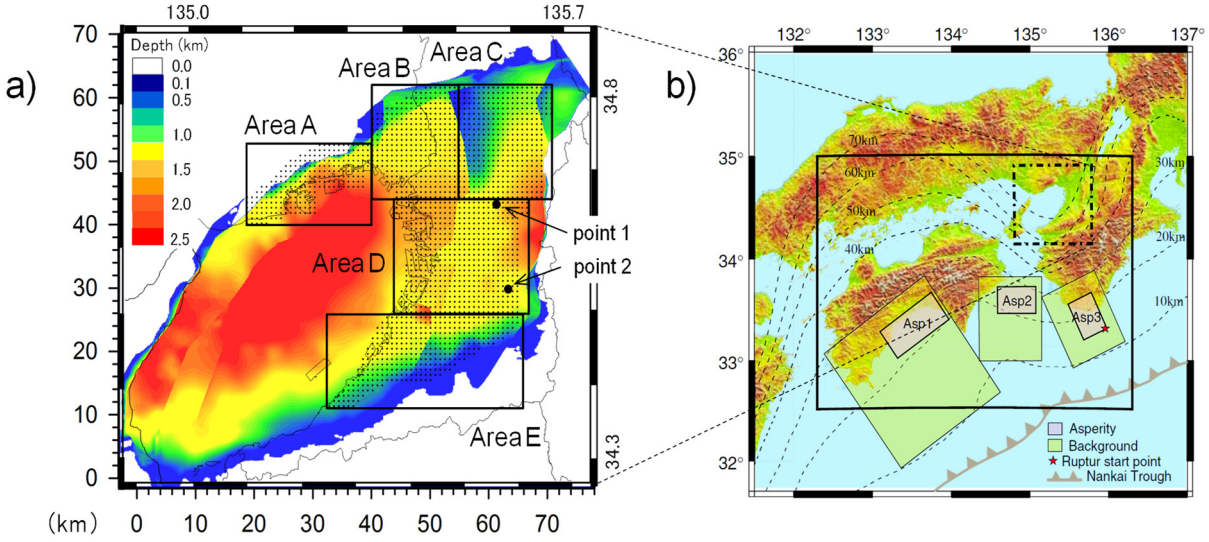

Fig. 4 The depth distribution of basin-bedrock interface for Osaka sedimentary basin model (a) and focal region of hypothetical Nankai earthquake (b).

influences indications of strong ground motion in the long-period band, was taken as the southeastern corner of Asp3.

Fig. 5 shows the maximum velocity distributions of the north-south and east-west components of the input ground motion. The maximum velocity distributions vary significantly from region to region in the Osaka plain. In particular, larger values are seen from the center of Osaka Bay to the Port of Kobe (southern side of Area A); as shown in Fig. 4b, this is affected by incoming waves that are amplified as they propagate through the thick sedimentary layers of Osaka Bay[19]. In all regions, the north-south component is larger than the east-west component, largely due to the S-wave radiation properties of Asp3. For the purposes of the following discussion, we divide the Osaka plain into 5 areas (Areas A–E) and restrict the focus of our analysis to north-south components only. As a summary of the frequency characteristics of input ground motion in each area, Fig. 6 shows pSv (h=5%) for periods in the range of 2-6 s. The value exceeds 200 cm/s for periods in the range of 2-5 s in Area A, a period of 2 s in Area B and the eastern portion of Area C, periods in the range of 4-5 s in the center of Area D, and periods of 2 s and 4-5 s in Area E. This indicates that the radiation properties of the seismic sources described above, and the propagation pathways of waves through sedimentary layers, are significantly affected by period-dependent characteristics at each location[19]. Note that, in this paper, we are attempting to derive a common benchmark indicator for input ground motion that will be highly correlated with a building's maximum response to a single seismic source model at all points over a plain. Ground motion at *specific* sites will be affected by fluctuations in the source model, but these fluctuations will be less significant than fluctuations in ground motion due to a specific source model over the entire region of the plain. Consequently, we expect that fluctuations in earthquake-source models will have minimal impact on the benchmark indicator derived in this paper.

3.2 Relationship between pSv and PIDR

Fig. 7 shows the relationship between PIDR values at all sites, arising from the input ground motion discussed in the previous section and obtained via analysis of the equivalent SDOF system in the elasto-plastic regime, and the pSv value at the same period of 2 s as the natural period corresponding to the initial stiffness (T_0). Fig. 8 plots PIDR vs. the ratio of the natural period in elasto-plastic response to the natural period at the initial stiffness (T_{eq}/T_0) obtained from Fig. 2.

We can identify three distinct regimes in the relationship between pSv and PIDR.

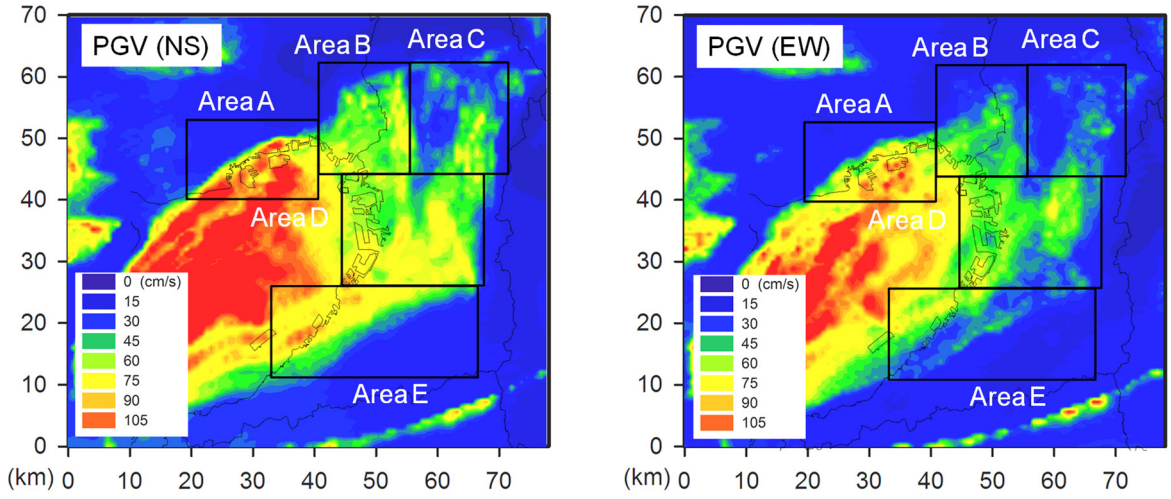

Fig. 5 Maximum velocity distribution of input ground motion waveforms
(left: north-south; right: east-west).

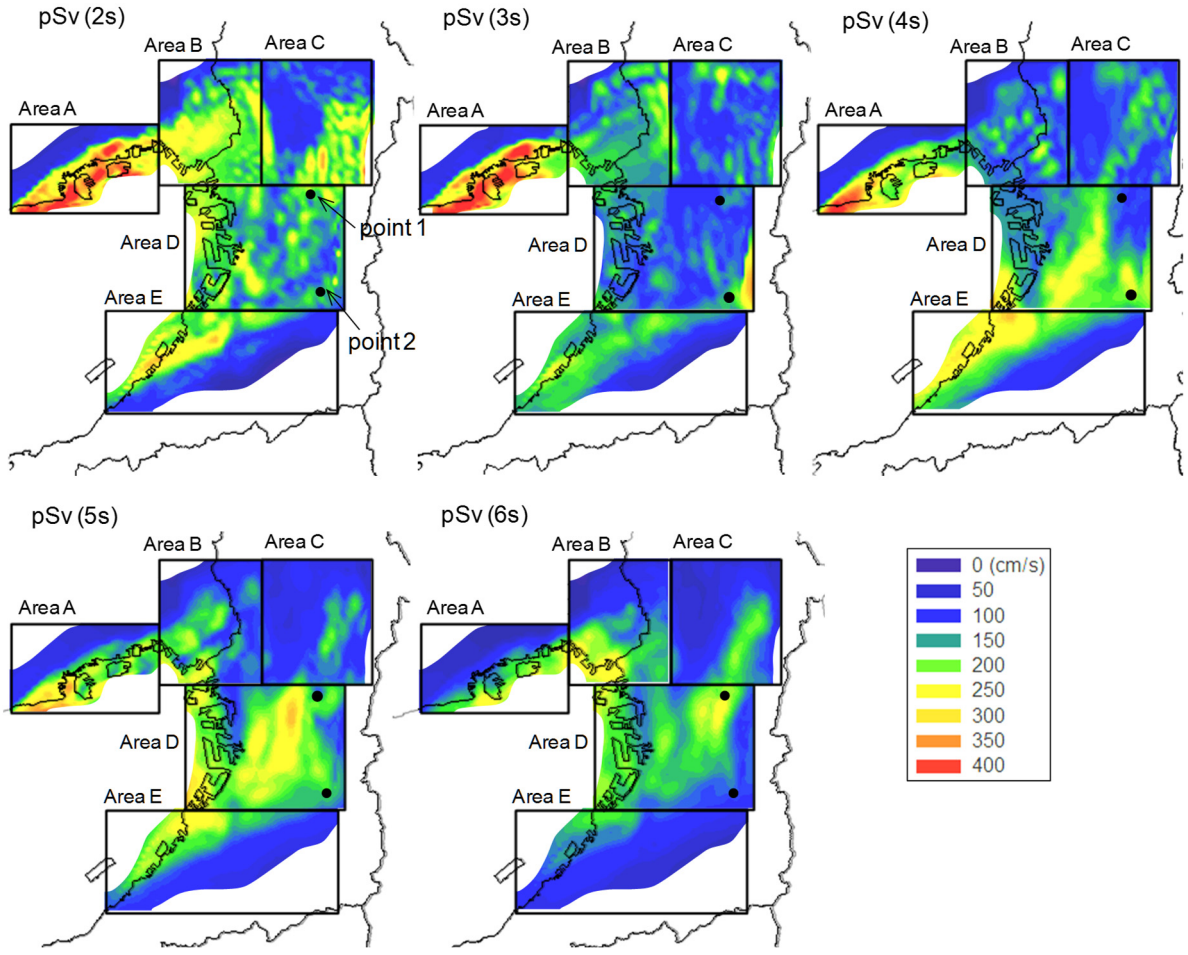

Fig. 6 Distribution of pseudovelocity response spectra (damping factor 5%)
for periods of 2, 3, 4, 5, and 6 s.

(1) From Fig. 7, we see that, for pSv less than around 50 cm/s or PIDR less than around 4×10^{-3}, the increase in the natural period is never more than a maximum of around 50%, as indicated by Fig. 8; thus, correlation with pSv is high regardless of location.

(2) For pSv>100 cm/s, fluctuations in PIDR values are large and correlations are small. This is because, as the input ground motion level increases in relative terms, the increase in natural period due to stiffness degradation becomes more prominent, and thus the PIDR depends on the amplitude characteristics over a wide range of periods (up to a maximum of around 2.5 T_0, judging from Fig. 8), which differ from site to site.

(3) As a transition state from regime **(1)** to regime **(2)** the PIDR correlation in the range of 50<pSv <100 cm/s decreases dramatically compared to what is observed at lower pSv values [regime **(1)**]. PIDR values at many points in this interval fluctuate in the range of 5<PIDR<10 ($\times10^{-3}$). This is because, as indicated by the two arrows in Fig. 8, the PIDR in this regime varies more sensitively with variations in natural period. To inspect regime **(2)** here, Fig. 9a shows pSv for input ground motion for 6 sites in Area D at which the pSv is approximately 200 cm/s and the PIDR takes one of two values: $\sim8\times10^{-3}$ and $\sim13\times10^{-3}$. The blue and red curves correspond respectively for the smaller-PIDR and larger-PIDR groups. Fig. 9b shows velocity waveforms at representative points in each of the 6 sites (indicated by thick lines in Fig. 9a, corresponding to empty circles in the plot of Fig. 7). The pSv near a period of 2 s takes the same value at all sites, but the pSv for periods in the range of 3-4 s is up to about twice as large for the large-PIDR group as for the small-PIDR group. (For reference, we have indicated the locations of the representative points with filled circles in Figs. 4b and 6.) These results provide further evidence for the conclusions discussed above. This PIDR for high-rise RC structures in the large-amplitude regime (PIDR values around 1/200 or greater) is governed by the magnitude of the velocity response spectrum for input ground motion over a spectral bandwidth extending to the value of the elastic-response natural period after it has been increased due to stiffness degradation.

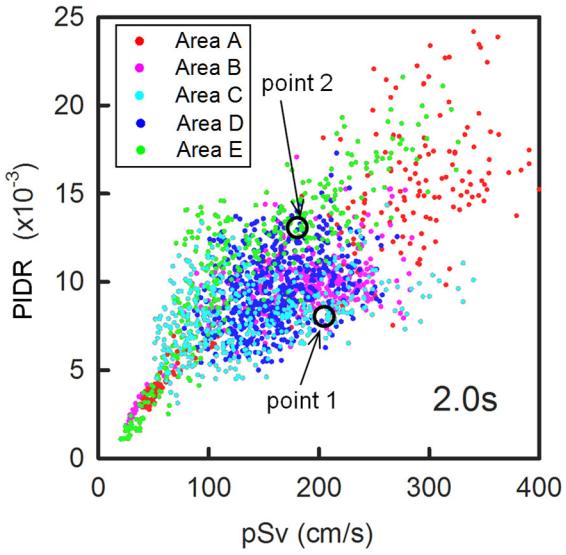

Fig. 7 Relationship between PIDR and pseudovelocity response spectra (period = 2 s) at all locations.

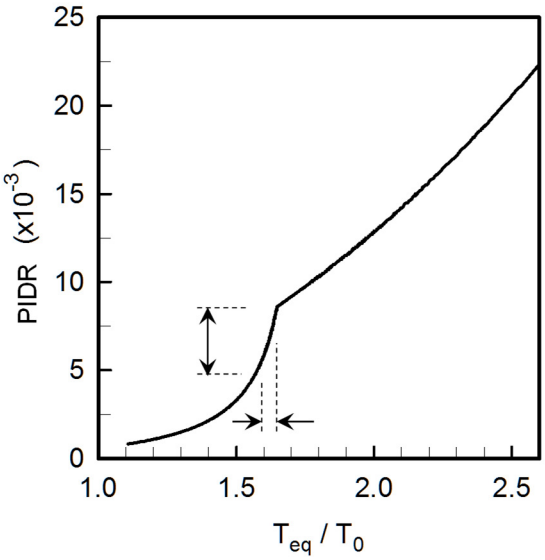

Fig. 8 Relationship between PIDR and natural period ratio for equivalent SDOF model.

3.3 Relationship between mean values of pSv and PIDR

A quantity that is frequently used to quantify numerically the impact of ground motion on the entirety of a building with various natural periods is the integral of the velocity response spectrum (h=20%) over the period range of 0.1-2.5 s, known as the *SI value*[20]. Also, Hida et al.[4], in a study of high-rise

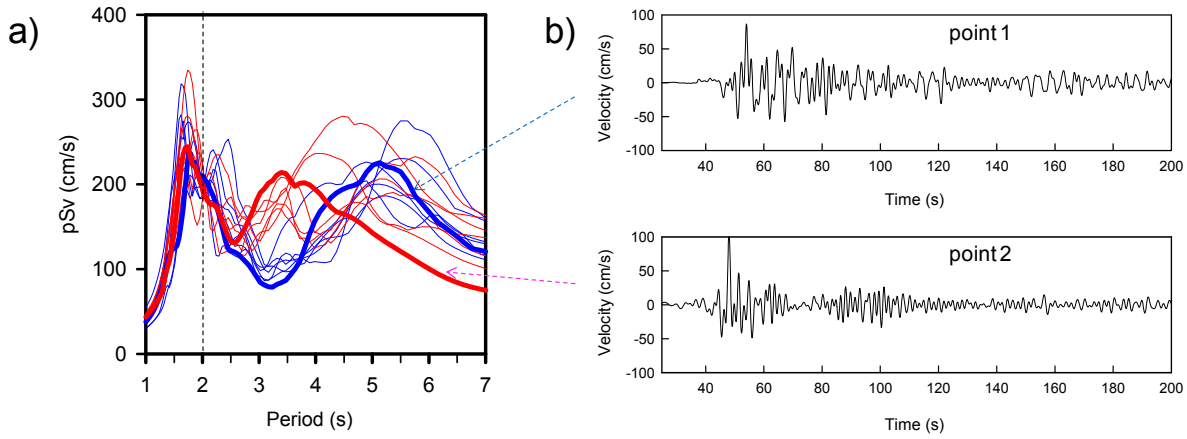

Fig. 9 Pseudovelocity response spectra for two groups of buildings with differing PIDR magnitudes (a) and input ground motion velocity waveforms at representative points in each group (b).

RC buildings in the Kanto region during the Tohoku-Oki earthquake, derived a relationship between PIDR and the mean value of the pSv (h=5%), observed at the base of the building, over the period range of 1.5-3.5 s [Equation (2) with coefficients α, β obtained via regression analysis] for PIDR values less than around 6×10^{-3}. The basic form of this equation is similar to the quadratic function for velocity response spectra by Okano et al.[21].

$$\gamma = (\alpha\ \overline{pSv} + \beta)^2 \times 10^{-3} \quad (2)$$

Here, $\overline{pSv}$ indicates the mean value of the pSv over a given range of periods.

Also, Kanda et al.[22] used waves predicted for a hypothetical Nankai-trough earthquake—together with the relationship of the spectrum of maximum absolute velocity response to input ground motion, and the mean value of the maximum energy spectrum over a range of periods to response quantities such as the PIDR obtained from a high-rise-steel-structural model or the integrated plastic deformation magnifier—to compute a benchmark indicator of building swaying motion from input ground motion. Based on these previous studies, here we use the quantity pSv (h=5%)—which we also used to establish criteria for indicated spectra in the long-period band (Fig. 1b), and which is also frequently used to assess the strength levels of input ground motion in the long-period band—to derive a benchmark indicator obtained from input ground motion (the quantity most highly correlated with the PIDR of high-rise RC structures) by analyzing response levels over a wide range, as far as the third branch of skeleton curves.

Figs. 10a-c show the relationship between PIDR and mean pSv value over three period bands: 2-3 s, 2-4.5 s, and 2-6 s of the natural period at the initial stiffness. For the narrowest band (Fig. 10a) in the range of mean pSv values near 50 cm/s, the correlation with PIDR is high, and we see a trend similar to that of Fig. 7 discussed earlier. For mean pSv greater than 150 cm/s, we see that the plots for Area B and Area E tend to separate and that plots for Area D tend to exhibit large fluctuations. For the broadest band (Fig. 10b), the PIDR fluctuations seen for mean pSv > 200 cm/s are smaller than in Fig. 10a, but the fluctuations at other mean pSv values are as large as those of Fig. 10a. For this reason, we also plot values for the bands 2-4.5 s (Fig. 10c) and 2.5-4.5 s (Fig. 10d); note that 2.5 s, which corresponds to $T_{eq}/T_0\approx1.25$ in Fig. 8 (here we have T_0=2 s), corresponds to a PIDR of 2×10^{-3}, the value at which interior materials begin to suffer damage[4]. We see clearly that correlations in these figures are higher than in the cases of Figs. 10a,b. In addition, in Fig. 10d, the fluctuations in the regime of 100 cm/s and above are reduced compared to Fig. 10c.

We next derive a regression equation relating the mean pSv to PIDR for the scatter plot of Fig. 10d. For our regression analysis, we use values in the range of 50 < mean pSv < 250 cm/s; this is because

mean pSv samples below 50 cm/s exhibit trends that differ from those of samples at higher values, and because samples with mean pSv in excess of 250 cm/s are distributed in the ocean regions of Area A (Fig. 4b). Nearly 95% of all samples are included in this range (Fig. 11a; for reference we also show in Fig. 11b the integrated frequency distribution of PIDR values resulting from our response analysis). The regression equation of Hida et al.[4)], which was derived from observational data with mean pSv values in the range of 1.5<pSv<3.5 s and PIDR values below 6×10^{-3}, is indicated by the dashed curve in Fig. 10a; among the plots of Figs. 10a-c, the spectral band used to compute the mean pSv corresponds most closely to the analysis of Ref. 4. This curve agrees well with the sample plot in the regime of relatively small PIDR (or relatively small mean pSv) in the same figure.

Now we discuss our procedure for deriving values for the regression parameters. From the regression equation derived by Hida et al.[4)], at a mean pSv=50 cm/s we find PIDR=3.5×10^{-3}. Next, in the regression equation [the functional form relating γ to mean pSv in equation (2)] we shift the origin to the initial value of the mean pSv in the defining region (50 cm/s) and define the new independent variable mean pSv' in this new coordinate system according to mean pSv' = mean pSv – 50. Then, we determine the parameter β' in the new coordinate system so that the new independent variable takes the value 0 at a γ(PIDR) value of 3.5×10^{-3}. The only remaining regression parameter in the new coordinate system is α, so we can perform a nonlinear regression analysis on our samples to determine its value.

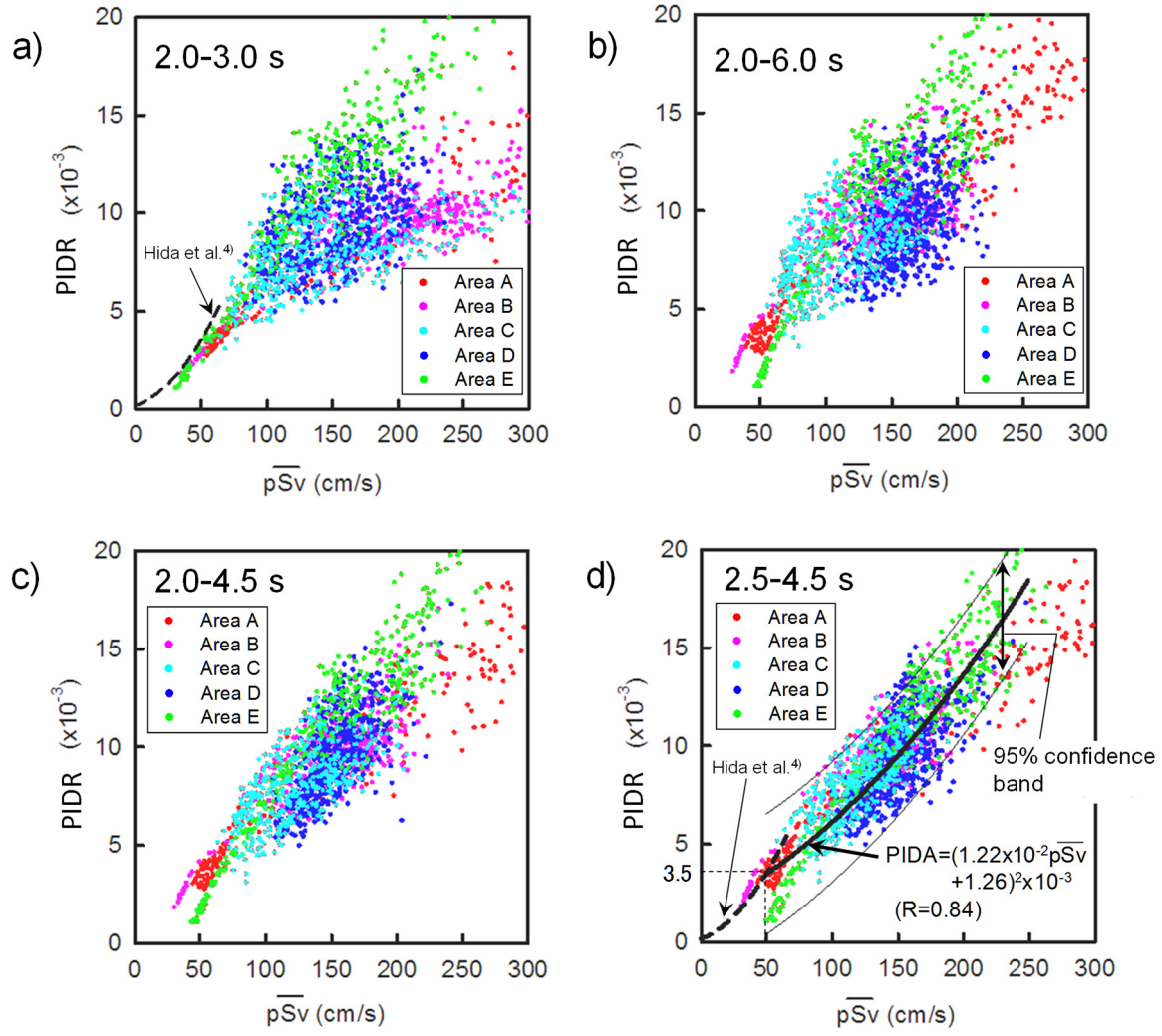

Figure 10: Relationship between PIDR and pseudovelocity response spectra averaged over four spectral bandwidths; (a) 2.0-3.0 s, (b) 2.0-6.0 s, (c) 2.0-4.5 s, (d) 2.5-4.5 s.

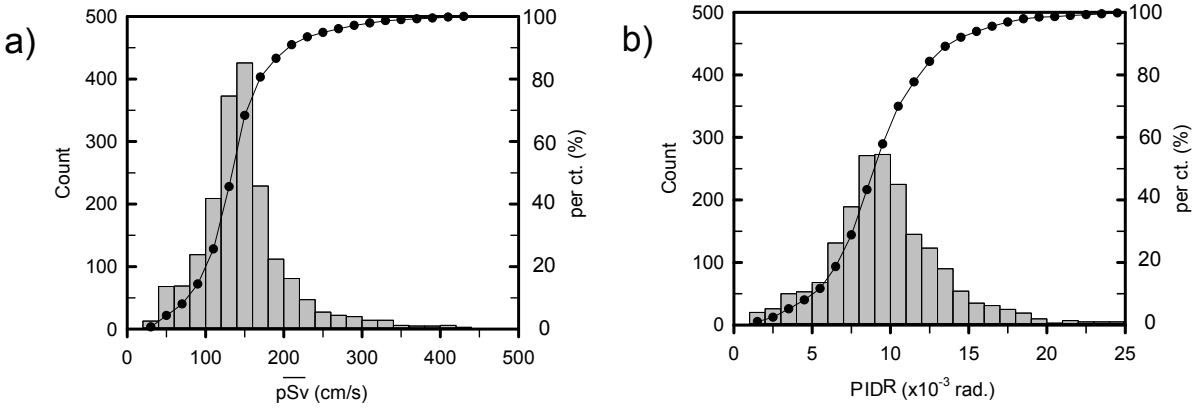

Figure 11: Histogram and fractional totals of (a) pseudovelocity response spectra averaged over the band 2.5-4.5 s, (b) PIDR values for all samples.

In searching for parameter values, we use the Marquardt-Levenberg algorithm[23], which minimizes the mean square sum of the residuals between the predicted and actual values of the dependent variable (PIDR). Finally, we shift back from the new coordinate system to the original coordinate system to determine the two parameters in equation (2). This yields the values $\alpha=1.22\times10^{-2}$ and $\beta=1.26$ (correlation coefficient R=0.84). The 95% confidence interval for the regression curve obtained is shown with thick solid lines and thin solid lines in Fig. 10. Note that, because the number of samples is extremely large, the 95% confidence interval differs from the regression curve by only a tiny amount. As noted above, in this work we focus on input ground motion with mean pSv of 50 cm/s or greater; in contrast, Hida et al.[4] focused on the regime of around 50 cm/s or less (Fig. 1b) for the Kanto region in the Tohoku-Oki earthquake. The buildings considered in the inductive process for the equation of Hida et al.[4] have a variety of elastic natural periods, and thus the magnification factor that should be applied to the spectral bandwidth over which mean pSv is calculated differs from building to building, making rigorous comparison difficult; however, Fig. 10 (a or d) agrees reasonably well with the analytical results (scatter plot) of this paper. Thus, by combining the two predictive equations with a crossover near the mean pSv value noted above, it may be provisionally possible to obtain predicted PIDR values over a wide range of input ground motion levels.

Fig. 12 shows contour maps illustrating the relationship between mean pSv and PIDR for Fig. 10d. We see that the distribution of colors agrees well between the two images. Also, for the hypothetical Nankai earthquake of Fig. 4a, the extent of damage to high-rise RC buildings with periods near 2 s tends to be large in the southern portion of Area A (coastal regions and landfill of Kobe City), the eastern portion of Area B (the lower side of the Uemachi fault), the coastal regions (landfill in Osaka City) and southern portion (Minami Kawauchi) of Area D, and the western portion of Area E (Senshu). This suggests that the oscillation period is not solely determined by the underground structure immediately beneath each site, but is also affected by the underground structure of propagation pathways for waves in the Osaka plain, as discussed above.

3.4 Characterizing structural models with different natural periods

The benchmark indicator in the previous section was derived for a model in which the natural period was 2 s. To what extent may this indicator be used to characterize structures with different natural periods? To investigate this question, we considered an equivalent SDOF model of an RC structure with T_0=3 s and studied the relationship between mean pSv and PIDR for Areas A, D, and E, which exhibit relatively large fluctuations among the 5 areas in the scatter plot of Fig. 10[24]. The results are plotted in Fig. 13. Here, the band over which we computed the mean pSv was 3.75-6.75 s, which was chosen to ensure the same value of the ratio T_{eq}/T_0 (1.25-2.25) used in previous sections. The curve in

Fig. 13 is for the regression equation previously derived for the case T_0=2 s; we see a high correlation with the data samples. Thus, we conclude that the benchmark indicator (regression equation) derived in this paper may be applied to RC structures with other natural periods simply by choosing the magnifiers appropriately (as in the brackets given above) when computing mean pSv values.

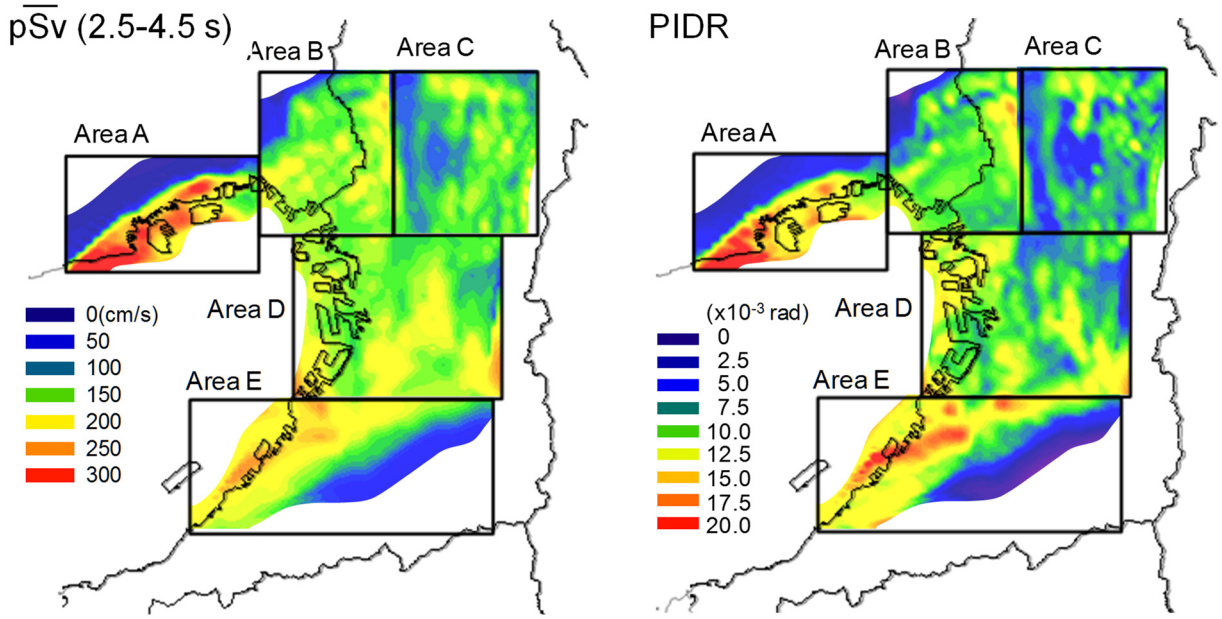

Figure 12: Correspondence between geographical distributions of mean pseudovelocity response spectra (left) and PIDR values (right).

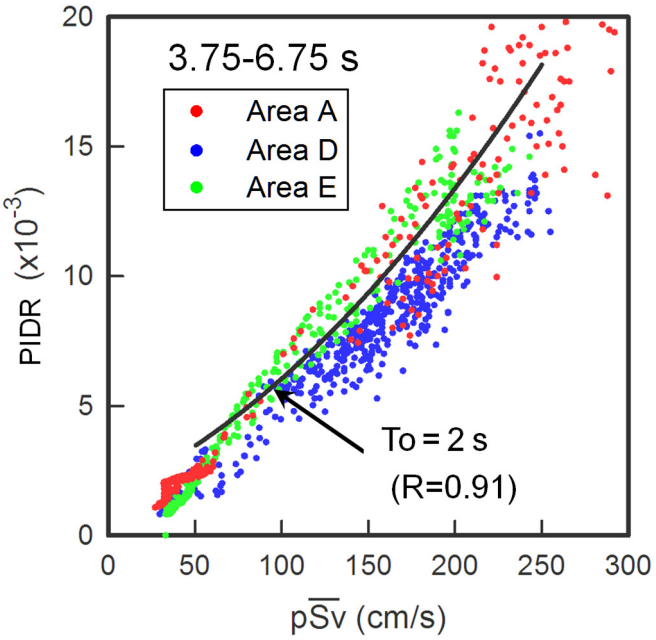

Figure 13: Relationship between PIDR and mean pseudovelocity response spectra for an equivalent SDOF system with natural period of 3 s.

4. CONCLUSIONS AND DISCUSSION

For a large number of high-rise RC structures for which strong-motion measurements or observations of microtremors before and after earthquakes have not been carried out, we obtained a benchmark indicator (a regression equation) allowing simple characterization—based on pseudovelocity response spectra (pSv) for input ground motion estimated from strong-motion records measured at ground points closed to the building, as well as re-created waves and other data—of peak inter-story drift ratio (PIDR averaged over all stories) values expected in a future major earthquake. The assumptions and main results of this paper are as follows.

1) PIDR is strongly correlated with the mean value of the pSv (h=5%) for input ground motion averaged over a spectral band of width 1.25-2.25 times the natural period of the initial stiffness.
2) Considering a hypothetical Nankai earthquake, and using data (a scatter plot) relating mean pSv values for predicted waves at 1,868 sites obtained from a model of the Osaka sedimentary basin to PIDR values determined by analysis of response to predicted waves using an equivalent elasto-plastic SDOF model, we used a regression analysis based on an equation expressing PIDR as a quadratic function of mean pSv to obtain a benchmark indicator relating PIDR to mean pSv.
3) Skeleton curves for the equivalent elasto-plastic SDOF model, and their dynamic properties, were determined based on design data and strong-motion records for 13 high-rise RC structures in the Hyogoken-Nambu and Tohoku-Oki earthquakes.
4) The relationship between PIDR and pSv at the natural period corresponding to the initial stiffness consists of the following 3 regimes.
   i) For pSv < approximately 50 cm/s, the natural-period enhancement is less than a maximum of around 50%, so PIDR is highly correlated with mean pSv in this regime.
   ii) For pSv > 100 cm/s, the natural-period enhancement is more pronounced and is affected by input seismic data over a broader spectral band, with considerable variation from site to site; as a result, the PIDR exhibits large fluctuations and is only weakly correlated with pSv.
   iii) The transition between regimes i) and ii) occurs rapidly over the range of 50 < pSv < 100 cm/s. This is because responses corresponding to this range are located on the second branch of the skeleton curve near the second inflection point ($5\times10^{-3}<PIDR<10\times10^{-3}$), where the PIDR is most sensitive to changes in the natural period.
5) For the Osaka plain in a hypothetical Nankai earthquake, pSv values in the period range of 2-5 s—which contribute significantly to the damage incurred by high-rise RC buildings—are largest in extremal regions, such as landfill regions of Kobe, which are heavily affected by waves that arrive after propagating through thick sedimentary layers at the center of Osaka Bay. For this reason, the extent of damage suffered by high-rise RC buildings is also greatest in those regions.

In closing, we make two observations.

1) Using the benchmark indicator derived in this work is equivalent to estimating the mean extent of damage (PIDR) for all stories. On the other hand, the extent of damage suffered by individual stories may be determined relatively easily by scaling PIDR values obtained from primary modes determined at design time or via load-increase analysis by the value predicted by our benchmark indicator for the mean PIDR over all stories. Note that the ratio of the maximum PIDR exhibited by any one story (typically intermediate stories) to the mean PIDR averaged over all stories is typically thought to lie approximately in the range of 1.5–2[15].
2) The equation (indicator) we derived in this paper is applicable for mean pSv values of 50 cm/s or above. For input ground motion levels around this value and below, we have adjusted our model to ensure agreement at 50 cm/s with the equation proposed by Hida et al.[4]. Thus, by combining these two equations, it is likely that PIDR values may be predicted over a wide range of input ground motion levels.

ACKNOWLEDGMENTS

We are grateful to Toda Corporation and to the Urban Renaissance Agency for providing observational records and building information. We used observational records taken from Refs. 12, 13. We are also grateful to Science Technology Inc. (Representative director: Dr. Osamu Uchida) for assistance with the response analysis.

REFERENCES

1) Nakayama T. and Hashimoto S.: An Inquiry into Markets and Supplies with Reference to the Statistics in the High-Rise Buildings, *Summaries of Technical Papers of Annual Meeting*, Architectural Institute of Japan, B-2, pp. 1405–1406, 2011. (in Japanese)
2) Cabinet Office Japan, Disaster Management in Japan: http://www.bousai.go.jp/jishin/nankai/nankaitrough_report.html. (in Japanese, last accessed in December 3, 2017)
3) Cabinet Office Japan, Disaster Management in Japan: Special Expert Study Group on Tonankai and Nankai Earthquakes: *The 16th Material 2*, http://www.bousai.go.jp/kaigirep/chuobou/senmon/tounankai_nankaijishin/16/index.html. (in Japanese, last accessed in December 3, 2017)
4) Hida T. and Nagano M.: Study on Shaking and Damages of Super High-Rise Residential Buildings during the 2011 off the Pacific Coast of Tohoku Earthquake based on Questionnaire Survey, *Proceedings of the 15th World Conference on Earthquake Engineering*, Lisbon, Portugal, 2012.
5) Uebayashi, H., Nagano M., Hida T., Tanuma T., Yasui M. and Sakai S.: Evaluation of the Structural Damage of High-Rise Reinforced Concrete Buildings using Ambient Vibrations Recorded before and after Damage, *Earthquake Engineering and Structural Dynamics*, 45, pp. 213-228, 2016.
6) Kimura T., Tanaka M., Konoue N., Nakamura M. and Kusakabe K.: Analytical Studies on the Behavior of a High-Rise SRC Building at Shin-Nagata during the Hyogo-Ken Nanbu Earthquake: Part 1 Outline of the Building and the observed Earthquake Motion, *Summaries of Technical Papers of Annual Meeting*, Architectural Institute of Japan, B-2, pp. 533–534, 1996. (in Japanese)
7) Housing and Urban Development Corp. (The urban renaissance agency at current) and Konoike Cons. Co. Ltd.: *Investigation Report*, On Earthquake Resistance on the High-Rise RC Apartment Housing at Takami subjected to the 1995 Hyogo-Ken Nanbu Earthquake based on the Record by Earthquake Observation, 1996, http://ci.nii.ac.jp/ncid/BB02756596?l=ja. (in Japanese, last accessed in December 3, 2017)
8) Nakamura M., Yasui Y., Wakamatsu K. and Nobata A.: A Study on Evaluation for Restoring Force Characteristics based on Earthquake Records; Restoring Force Characteristics at a 41-Stories RC Building before and after the Hyogo-Ken Nanbu Earthquake, *Summaries of Technical Papers of Annual Meeting*, Architectural Institute of Japan, B-2, pp. 445–446, 1995. (in Japanese)
9) Nagano M., Hida T., Tanuma T. and Watanabe K.: Dynamic Nonlinear Response of Super High-Rise Residential Buildings in Urbanized Area during the 2011 off the Pacific Coast of Tohoku Earthquake, *Proceedings of the 15th World Conference on Earthquake Engineering*, Lisbon, Portugal, 2012.
10) Japan Seismic Isolation Association: *Committee Report*, Response Control Building Investigation, 2012.
11) Uebayashi, H. and Nagano M.: Evaluation of Amplification Characteristics and Dynamic Properties of Skyscrapers based on Strong Motion Records, *Journal of Technology and Design*, Architectural Institute of Japan, 19(42), pp. 435-440, 2013. (in Japanese with English abstract)
12) The former Association for Earthquake Disaster Prevention: Strong Motion Data by 16 Agencies and the University of Tokyo Strong Motion Array during the 1995 Kobe Earthquake, Provided by *Japan Association for Earthquake Engineering*, 1996. (revised version)
13) Hisada Laboratory, Kogakuin University: http://kouzou.cc.kogakuin.ac.jp/newhp/open_data.html. (in Japanese, last accessed in December 3, 2017)
14) Nakagawa, Y., Kawabe, H. and Kamae, K.: Long-Period Ground Motion Prediction and High-Rise

Buildings Response in the Osaka Basin for Future Nankai Earthquake, *Proceedings of the 37th Symposium of Earthquake Ground Motion*, Architectural Institute of Japan, pp. 89-96, 2009. (in Japanese with English abstract)
15) Yamane Y., Nagano M., Hida T., Yasui M., Yamamoto T., Ikawa N. and Tanuma T.: Study on Real Indoor Damages of Super-High-Rise Residential Buildings during the 2011 off the Pacific Coast of Tohoku Earthquake related with Structural Responses, *Journal of Technology and Design*, Architectural Institute of Japan, 20(44), pp. 67-72, 2014. (in Japanese with English abstract)
16) Yamada, A. and Kanayama, H.: Study and Application of Strength Demand for Steel Structures, *Summaries of Technical Papers of Annual Meeting*, Architectural Institute of Japan, B-2, pp. 973-974, 1997. (in Japanese)
17) Yamane Y., Nagano M., Hida T. and Tanuma T.: Height-Wise Distribution of Maximum Inter-story Drift Angles in Super High-Rise RC Buildings based on Earthquake Response Analysis Models for Structural Design, *Journal of Technology and Design*, Architectural Institute of Japan, 22(50), pp. 93-98, 2016. (in Japanese with English abstract)
18) Kawabe, H. and Kamae, K.: Prediction of Long-Period Ground Motions from Huge Subduction Earthquakes in Osaka, Japan, *Journal of Seismology*, 12, pp. 173-184, 2008.
19) Uebayashi, H., Kawabe, H. and Kamae, K.: Amplification Characteristics of Long-Period Ground Motions in Osaka Sedimentary Basin; Consideration based on Observed and Predicted Ground Motions, *Proceedings of the 40th Symposium of Earthquake Ground Motion*, Architectural Institute of Japan, pp. 87-100, 2012. (in Japanese with English abstract)
20) Housner, G.W.: Behavior of Structures during Earthquakes, *Proceedings of American Society of Civil Engineer*, EM4, Oct. 1959.
21) Okano, H. and Miyamoto, Y.: Equations derived from Equivalent Linearization Method; Consideration based on Energy Balance and its Application to Evaluation of Probability of Excess of Deformation Capacity, *Journal of Structural and Construction Engineering*, Architectural Institute of Japan, 67(562), pp. 45-52, 2002. (in Japanese with English abstract)
22) Kanda, K., Abe, M., Suzuki, Y., Fujiwara, H., Morikawa, N., Maeda, T., Koshika, N., Okano, H. and Kato, K.: Intensity Scales of Long-Period Ground Motions correlated with Structural Responses of High-Rise Buildings, *Journal of Structural and Construction Engineering*, Architectural Institute of Japan, 79(696), pp. 267-274, 2014. (in Japanese with English abstract)
23) Press, W. H., Flannery, B. P., Teukolsky, S. A. and Vetterling, W. T.: Numerical Recipes, *Cambridge University Press*, 1986.
24) Akizuki, M.: Study on Damage Indicator by Long-Period Ground Motion, *Master's Thesis of Socio-Environmental Energy Science*, Graduate School of Energy Science, Kyoto University, February, 2010. (in Japanese)

(Original Japanese Paper Published: April, 2016)
(English Version Submitted: Dec 5, 2017)
(English Version Accepted: Apr 26, 2018)